

Structured light with a million light planes per second

Dhawal Sirikonda^a, Praneeth Chakravarthula^b, Ioannis Gkioulekas^c, Adithya Pediredla^a
^aDartmouth College, ^bUNC Chapel Hill, ^cCarnegie Mellon University

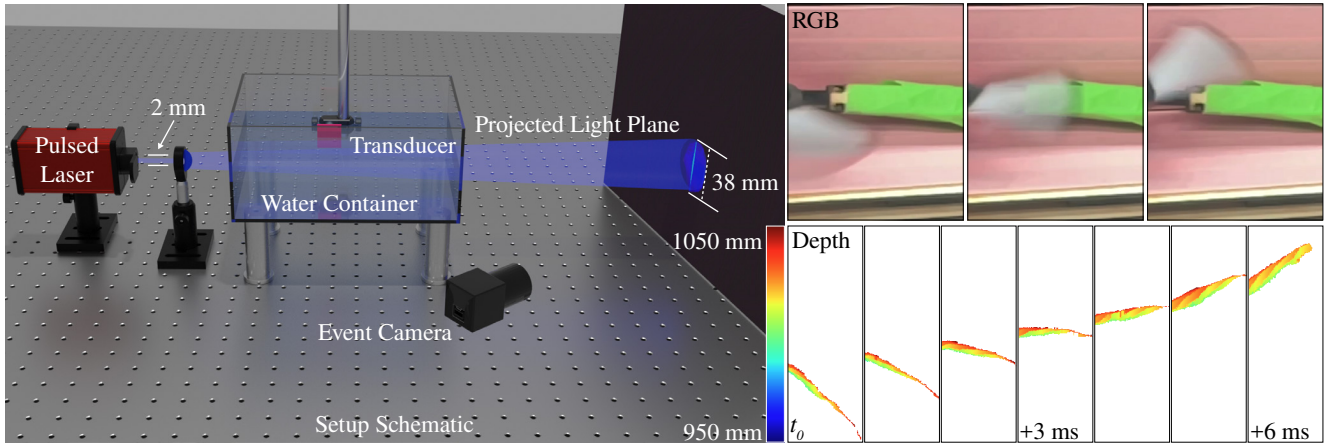


Figure 1. We present a structured light technology that combines acousto-optic light scanning with an event camera for high-speed operation. Left: Schematic of our setup. We use an ultrasonic transducer to sculpt virtual gradient-index cylindrical lenses inside a transparent medium (water). Coupling this medium with pulsed illumination, we can scan the scene with a light plane at speeds three orders of magnitude faster than the event camera’s, allowing structured light operation at the camera’s full-frame bandwidth. Right: To demonstrate the speed of our technique, we show reconstructed depth frames from a fan rotating at 1800 rpm scanned at 1000 fps. We also show for reference an RGB capture of the fan at 240 fps, illustrating the significant motion blur due to the fan rotation.

Abstract

We introduce a structured light system that captures full-frame depth at rates of a thousand frames per second, four times faster than the previous state of the art. Our key innovation to this end is the design of an acousto-optic light scanning device that can scan light planes at rates up to two million planes per second. We combine this device with an event camera for structured light, using the sparse events triggered on the camera as we sweep a light plane on the scene for depth triangulation. In contrast to prior work, where light scanning is the bottleneck towards faster structured light operation, our light scanning device is three orders of magnitude faster than the event camera’s full-frame bandwidth, thus allowing us to take full advantage of the event camera’s fast operation. To surpass this bandwidth, we additionally demonstrate adaptive scanning of only regions of interest, at speeds an order of magnitude faster than the theoretical full-frame limit for event cameras.

1. Introduction

3D scanning is the process of capturing the detailed geometry of real-world objects, using methods such as time of flight, structured light, or photogrammetry. 3D scanning is particularly useful for dynamic scenes, where real-time 3D information allows for accurate analysis of moving objects. For instance, scanning moving surroundings enhances navigation and safety in autonomous driving and robotics, and enables interactive experiences in virtual and augmented reality. 3D scanning is also crucial in industrial manufacturing environments, for inspection of objects in fast motion. All these applications require *fast* 3D scanning that minimizes motion blur and other motion-induced artifacts.

Fast 3D scanning necessitates high-speed light sources, using for example Galvo projectors as in advanced lidar systems, and high-speed cameras, such as single-photon avalanche diodes (SPADs) or event sensors. In conjunction with this hardware, it requires efficient algorithms to process and filter data rapidly, handling tasks such as noise reduction, data fusion, and reconstruction. In scanning systems that uti-

lize multiple sensors, synchronization of sensors also plays a crucial role in ensuring coherent data capture and integration from different sources. Unfortunately, fast 3D scanning methods are limited to rates below 1000 fps, primarily due to constraints imposed by the scanning speeds of existing light scanning systems: Though fast imaging sensors such as event cameras exist, light scanning systems are limited to scan rates of a few kHz, falling well short of fully exploiting the fast sensor readout.

In this work, we push the envelope of achievable 3D scanning speeds, by designing an ultra-fast structured light (SL) system that combines an acousto-optic (AO) light scanning device and an event camera. The AO device comprises a pulsed laser and an ultrasonic transducer. The transducer generates an ultrasonic wave that sculpts traveling virtual cylindrical lenses in a water medium. These lenses focus the laser light onto a line. By steering these cylindrical lenses at MHz rates, we can scan the line over a 3D scene imaged by the event camera, enabling structured light scanning. The AO device uses a design that results in an order-of-magnitude cost reduction relative to prior such devices [44].

Our AO device achieves light scanning rates that are more than three orders of magnitude higher than the frame rate of the event camera. When used for structured light, our device shifts the bottleneck towards higher speeds from the scan rate of the light device to the readout bandwidth of the imaging sensors. To further improve speed beyond this bottleneck, we demonstrate an adaptive method inspired by Muglikar et al. [36] to scan only regions of interest. Doing so boosts the capture frame rate by $10\times$ compared to the theoretical full-frame bandwidth limit of the event sensor. We build a benchtop prototype, and characterize its performance by scanning various static and dynamic scenes. In summary, we make the following contributions:

- Ultra-fast MHz rate line scanner based on a custom cost-effective acousto-optic setup.
- Fastest (up to 1 kfps) structured light depth-scanning rates reported so far (Table 1).
- Adaptive scanning method to scan beyond the limitations of event camera at 10 kHz scan rates.

2. Prior Work

Light scanning. Light scanning is a core component of active imaging technologies, including lidar [69], structured light [14, 57], light-transport probing [2, 37–39], motion contrast 3D [33], light curtains [8, 62], slope-disparity gating [9, 24, 61], and non-line-of-sight imaging [27, 30, 40, 43, 66]. We can broadly classify the light scanning methods in these technologies into mechanical and non-mechanical. Mechanical methods require moving parts such as rotating prisms [1, 64] or mirrors [22, 34], and micro-electromechanical systems (MEMS) [48, 52]. These meth-

Table 1. Scan speed comparison against recent works.

Work	Static	Dynamic
Muglikar et al. [35]	60 fps	60 fps
Matsuda et al. [33]	60 fps	60 fps
Dashpute et al. [11]	250 fps	30 fps
Ours	1 kfps	1 kfps

ods are slow due to mechanical inertia. Non-mechanical methods require no moving parts, and include acousto-optic (AO) [12, 68] and electro-optic (EO) [54] devices, liquid crystal devices (LCDs) [50, 63], and optical phased arrays (OPAs) [17, 46]. LCDs are the slowest of these methods due to long settling times. OPAs are the fastest and can scan light at even GHz rates, but have low angular resolutions, and thus are unsuitable for structured light. AO and EO devices provide a good middle ground, as we discuss next.

Light scanning with acousto-optic devices. Commercially available AO and EO devices include tunable filters [13], modulators [3], frequency shifters [70], and deflectors [19]. AO deflectors can serve as light scanning devices, but are limited to kHz scanning rates due to their reliance on Bragg’s diffraction [58]. EO deflectors [29, 53] operate on a similar principle, and thus are similarly slow. Alternative AO light scanning devices are tunable acoustic gradient-index (TAG) lenses [10, 20] and ultrasonically-sculpted virtual optical waveguides [7, 21, 44]—our technology is an instance of the latter. TAG lenses can change the focus depth of an incident beam at kHz rates, but cannot scan it transversely. By contrast, recent work [44] demonstrated transverse scanning at MHz rates using ultrasonically-sculpted virtual optical waveguides, motivating our work. Compare to the scanning system by Pediredla et al. [44], which phase-modulates the ultrasound for scanning, our system modulates the laser pulse. This adjustment allows us to use a *narrowband* amplifier, which is widely available and cost-effective (USD 250 instead of USD 23,000 for the broadband amplifier in Pediredla et al. [44]), reducing the overall system cost.

Event cameras and 3D sensing. Event cameras perform sparse readouts of relative intensity changes exceeding a pre-set threshold, and thus can achieve much larger frame rates than conventional cameras that always perform full-frame readouts. This high speed has made event cameras increasingly popular in computer vision [15, 59, 60]. Though extensive research exists for 2D imaging applications of event cameras, such as full-frame reconstruction [23, 28, 42, 47, 49, 51] and deblurring [16, 41, 55, 56, 67, 71], 3D imaging applications are still nascent. Brandli et al. [5] combined an event camera with a laser line scanner for structured-light 3D scanning, leveraging the fact that swept-plane structured light requires very sparse sensor readouts—only a column

Figure 2. Light plane formation and steering. (Video, viewable in Adobe Acrobat or GNU Okular.) A sinusoidal voltage applied to the planar transducer in Figure 1 generates a series of cylindrical GRIN lenses, which propagate at the speed of sound. By programming the timing of the illumination pulses, we can control the movement of the light planes focused through these lenses at specific speeds. This demonstration is adapted from Pediredla et al. [44].

per projected light plane. More recent works perform structured light by combining event cameras with laser point projectors [32, 33, 35, 36] or digital light processing projectors [26, 31]. In all these works, light scanning is slower than the frame rate of the event camera, and thus the bottleneck preventing faster 3D scanning. We remove this bottleneck by using a laser-line scanning system that combines acousto-optic lens sculpting with a pulsed laser, to achieve megahertz-rate light scanning—three orders of magnitude faster than the theoretical frame-rate limit of an event camera, thus turning the camera into the bottleneck towards faster structured light. Additionally, we push further beyond this bottleneck by developing an adaptive scanning algorithm that enables structured light rates an order of magnitude faster than those theoretically possible with an event camera.

3. Method

Structured light (SL) methods triangulate depth by establishing stereo correspondences between an active light projector and a camera. In its most basic form, SL uses the projector to raster scan individual points [33, 35]. Using the epipolar geometry allows accelerating structured light while maintaining robust correspondences, by projecting a line (light plane in 3D) orthogonal to the epipolar lines. Methods using optical codes such as binary [45], Gray [6], sinusoidal [18], or XOR [14] reduce the number of projected light patterns, but are detrimental for the event camera case—approximately half the sensor pixels will be lit for each projected pattern, increasing the total number of events generated by the event camera and thus slowing the scanning rate.

Motivated by these considerations, we opt for a system that uses line projection and an event camera for structured light. We build an acousto-optic line scanning prototype that can project two million lines per second (lps), exceeding the event camera theoretical detection rate ($\approx 10^6$ lps), and being orders of magnitude faster than alternative pro-

jection systems used for structured light, including Galvo mirrors [11, 33], MEMS mirrors [26, 31], and laser projectors [32]. Below we describe the physical principles governing the operation of the line scanning device, and the algorithmic principles for programmable light scanning.

Ultrasonic sculpting of steerable lenses. The refractive index of an optical medium is a function of its density. By controlling a medium’s spatial density, we can control its spatially varying refractive index and convert the medium into a gradient-index (GRIN) lens. To this end, we use a planar acoustic transducer to create a pressure wave that sculpts inside a transparent medium (water) a cylindrical GRIN lens traveling at the speed of sound in that medium. Using this virtual cylindrical lens, we can focus a collimated beam of light onto a line that also moves at the speed of sound. We can then use this light beam for structured light.

If we apply sinusoidal voltage $V(t) = V_{\text{us}} \cos(2\pi f_{\text{us}} t)$ to the planar transducer at $x = 0$, the transducer will create ultrasound inducing a traveling pressure wave:

$$P(x, y, z, t) = P_0 + P_{\text{us}} \cos(2\pi/\lambda_{\text{us}} x - 2\pi f_{\text{us}} t), \quad (1)$$

where x, y, z are Cartesian coordinates, t is time, P_0 is the pressure in the medium without ultrasound, P_{us} is proportional to the input voltage amplitude V_{us} , and λ_{us} and f_{us} are the wavelength and frequency (resp.) of the ultrasound output by the transducer. The pressure wave creates a proportional change in the refractive index of the medium, resulting in a time-varying refractive index profile:

$$n(x, y, z, t) = n_0 + n_{\text{us}} \cos(2\pi/\lambda_{\text{us}} x - 2\pi f_{\text{us}} t), \quad (2)$$

where n_0 is the refractive index without ultrasound, and n_{us} is proportional to the pressure amplitude P_{us} . We drop y, z as the refractive index does not change along those axes. As Pediredla et al. [44] explain, each of the the convex lobes of $n(x, t)$ —corresponding to $x \in (k\lambda_{\text{us}} - \lambda/2, k\lambda_{\text{us}} + \lambda/2)$, $k \in \mathbb{Z}$ —acts as a cylindrical GRIN lens that travels along the x axis at the speed of ultrasound, $c_{\text{us}} = f_{\text{us}} \lambda_{\text{us}}$.

A light beam passing through this medium will focus onto a line—or series of lines if the beam width is larger than the ultrasound wavelength—traveling at speed c_{us} . Assuming for simplicity that the cylindrical lenses are aberration-free, the resulting intensity at the focal plane of the lenses is

$$I(x, t) = \sum_k \delta(x + k\lambda_{\text{us}} - c_{\text{us}} t), \quad (3)$$

up to a scale factor proportional to the illumination. Figure 2 visualizes the cylindrical lenses, focusing behavior of light rays, and their temporal dynamics.

Programmable control of light planes. The traveling cylindrical lens enables scanning a light plane, but does not provide a mechanism for controlling scanning speed. Consequently, the scanning rate of the light plane is faster than the

capture rate of the event camera. We overcome this problem by using a laser that we pulse at a controllable frequency. If this frequency is the same as the frequency of the ultrasound transducer, and assuming laser pulsation starts at $t = 0$, the light intensity at the focal plane will become:

$$I(x, t) = \sum_{k,l} \delta(x + k\lambda_{\text{us}} - l \underbrace{c_{\text{us}} T_{\text{us}}}_{\lambda_{\text{us}}}) \delta(t \bmod T_{\text{us}}), \quad (4)$$

where l indexes laser pulses, and the time $T_{\text{us}} = f_{\text{us}}^{-1}$ between two pulses equals the ultrasound period. Equation (4) describes a pulse train that does not translate in space but flickers in time at the ultrasonic frequency. Every l^{th} laser pulse illuminating the l^{th} period of the ultrasonic wave will generate a line at the origin ($x = 0$).

To move the lines spatially, we instead pulse the laser at a frequency slightly offset from the ultrasonic one. If α is the ratio of ultrasonic to laser frequency, Equation (4) becomes:

$$I(x, t) = \sum_{k,l} \delta(x + k\lambda_{\text{us}} - l\alpha\lambda_{\text{us}}) \delta(t \bmod \alpha T_{\text{us}}). \quad (5)$$

Therefore, when the l^{th} laser pulse illuminates the l^{th} period of the ultrasonic wave, the focused line will appear at $x = (1 - \alpha)l\lambda_{\text{us}}$ making the line move spatially from pulse to pulse. The line frequency is equal to the beat frequency $(1 - \alpha)f_{\text{us}}$ between ultrasound and laser.

Besides serial line scanning, our laser pulsing design allows us to place lines at a non-serial set of locations x_l ; $l \in \{1, 2, \dots, L\}$, simply by emitting laser pulses at times

$$T_l = \frac{x_l + l\lambda_{\text{us}}}{lc_{\text{us}}}. \quad (6)$$

This capability facilitates adaptive scanning of regions of interest, and in turn yet faster structured light rates (Section 5).

The above analysis assumed a collimated beam. If we use a diverging beam, the line scanning behavior remains the same, but the distance between the lines will increase. In our prototype, we use a diverging beam to increase the field of view of the structured light system, as we show in Figure 1.

Comparison to Pediredla et al. [44]. Our acousto-optic laser line scanning system is inspired by that introduced by Pediredla et al., with two important differences: 1. Pediredla et al. focus on point scanning for lidar applications, whereas we focus on line scanning for structured light. Therefore, their system uses two linear transducers, whereas ours using just one, effectively replacing spherical GRIN waveguides with cylindrical ones. 2. Pediredla et al. control the position of the focused spot by modulating the phase of the ultrasound, whereas we control the position of the focused line by pulsing the laser. The approach of Pediredla et al. creates two challenges: First, it requires using an expensive broadband RF amplifier (ENI-300L, USD 23,000), as the ultrasonic wave is no longer a monotonic sinusoid. Second, it requires that the transducers operate at non-resonant fre-

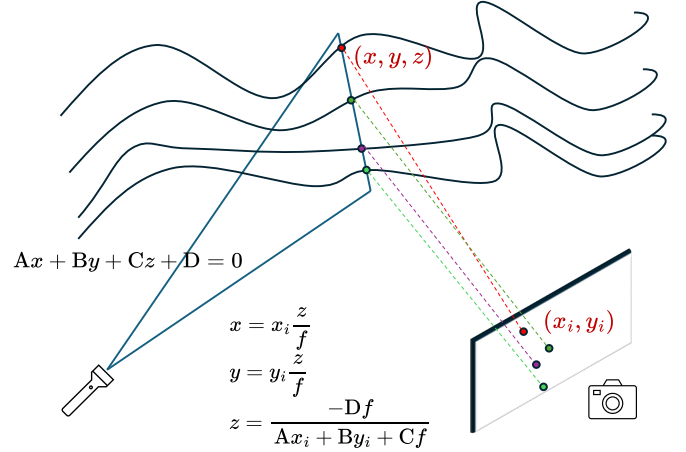


Figure 3. Structured light scanning with swept light planes. The light scanning device sweeps a light plane across the imaged scene. The reflected light triggers events at pixels along a vertical curve on the event camera. For each such pixel, depth is triangulated by intersecting a backprojected ray with the corresponding light plane.

quencies, where they consume more power. By contrast, our approach allows using a much less expensive narrowband amplifier (USD 250) and operating at lower power.

Structured light. For structured light, we use our AO light scanning device together with an event camera to form a stereo pair. We orient the planar transducer of our device such that the projected light planes are as orthogonal to the corresponding epipolar lines on the event camera as possible. By synchronizing the AO device and event camera, we can perform structured light scanning using the classical swept-plane procedure [4, 25], which we visualize in Figure 3: As the AO device scans a light plane, light reflected off the scanned object forms a vertical curve on the image plane that sweeps horizontally across the field of view, triggering sparse events (ideally one event per sensor row for each scan position, assuming perfect optics). From each such event, we can reconstruct a depth value for the corresponding pixel via triangulation, by backprojecting a ray and intersecting it with the light plane that triggered the event.

4. Hardware prototype

In this section, we detail hardware components and the system implementation. Figure 1 shows a schematic of the optical setup, and Figure 4 shows our hardware prototype.

Light scanning device. To implement the acousto-optic light scanner, we use an ultrasonic transducer of size $12.5 \text{ mm} \times 12.5 \text{ mm}$ tuned to operate at a 2 MHz frequency. We drive the transducer using a Siglent SDG 1032X arbitrary-waveform generator (AWG). We amplify the generator output using a narrowband RF amplifier (rated at 50 W and operating frequency 1 MHz to 3 MHz) before applying it to

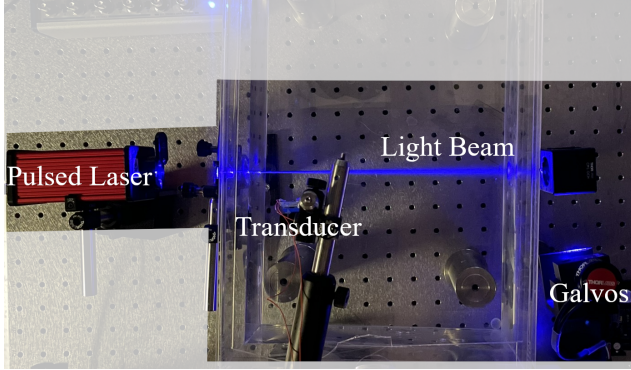


Figure 4. Hardware prototype for the schematic presented in Figure 1. We attach a Galvo mirror next to the water tank for comparisons, keeping the mirror static when we use AO scanning.

the transducer. For illumination, we use a Thorlabs NPL45B pulsed laser that we synchronize and drive using the AWG to achieve line scanning. We use a Thorlabs LA1274 40 mm convex lens to diverge the beam enough to cover the scanned scene. For comparison against existing steering techniques, we integrate a Thorlabs GVS211 single-axis Galvanometer into our system by placing a 45°-angle mirror in front of the light beam. When we use our acousto-optic light scanning, we keep the Galvo mirrors stationary.

Event camera. We use the Prophesee EVK-4 event camera, equipped with Sony’s IMX636 sensor. This sensor can process up to 1 GEvents/s, with events recorded at a temporal resolution of 1 μ s and spatial resolution of 1280 \times 720 pixels. As the horizontal axis has the fastest readout and provides timestamping, we orient this axis parallel to the light plane. This alignment allows us to utilize the event camera’s full bandwidth [35], corresponding to a maximum achievable frame rate of approximately $10^6/720 = 1388 \text{ Hz} \approx 1 \text{ kHz}$. We replace the default lens of the EVK-4 camera with a Rokinon DS50M-C full-frame lens of focal length 50 mm and speed $f/1.5$ to improve light efficiency during scanning.

We observed empirically that, with default settings, the event camera fails to capture events when sweeping light planes at frequencies higher than 100 Hz. To mitigate this problem, we set the camera’s parameters `bias-hpf` and `bias-refractory` to their maximum values, while completely removing the `bias-off` parameter, allowing a single polarity to utilize the complete bandwidth of the camera.

Synchronization. To synchronize events with the light planes that trigger them, one option is to use the event camera’s hardware trigger mechanism and synchronize with the AO light planes’ timestamps. However, at high-speed scanning when the event camera generates several events, we observed that this hardware synchronization mechanism fails. We thus develop a software-based synchronization system: We project light planes continuously and record them with

Table 2. Effect of scan rate on 3D reconstruction quality. (CD: chamfer distance in mm; F1: F1-score; Pr: precision; Re: recall.)

	fps	CD (\downarrow)	Pr (\uparrow)	Re (\uparrow)	F1 (\uparrow)
Cat	10	1.48	0.762	0.910	0.830
	100	1.25	0.812	0.953	0.877
	200	1.67	0.738	0.956	0.833
	1000	4.56	0.146	0.981	0.253
	1000 (acc.)	4.30	0.524	0.827	0.641
Dolphin	10	0.750	0.958	0.939	0.949
	100	1.273	0.961	0.817	0.883
	200	1.583	0.915	0.803	0.855
	1000	2.342	0.844	0.687	0.758
	1000 (acc.)	1.338	0.986	0.926	0.955

the event camera. We then use the event camera’s timestamp for the left-most line and the corresponding AO light plane’s time stamp for synchronization.

Geometric calibration. As our light scanning device is highly repeatable, we precalibrate scanned light planes through their linear intersections with two orthogonal reference planes, which we create using two LCD screens: We display blinking checkered patterns on the screens to calibrate the reference planes with respect to the event camera, then keep them turned off during structured light. We visualize this arrangement in the supplement. The whole procedure uses standard geometric calibration algorithms [4, 25].

5. Experiments and analysis

In this section, we systematically evaluate the performance of our proposed structured light system on static and dynamic scenes. We show that our system can reconstruct 3D scenes at the maximum frame rate of the event camera at a megapixel resolution. We also show an adaptive 3D scanning method that allows to selectively scan parts of the scene, thereby achieving a 10 \times higher frame rate. We empirically show that structured light systems using Galvo mirrors cannot effectively perform adaptive 3D scanning.

5.1. Static scene results

We first scan static scenes, to quantitatively and qualitatively evaluate the effect of scan rate on reconstruction performance. In Figure 5, we use two figurines as test objects for scanning. We first used Galvo-based SL at a slow speed (10 fps) to compute ground truth for comparison. We then used the AO device to scan the object at 10 fps, 100 fps, 200 fps, and 1 kfps scan rates. The figure shows the captured depth maps, and Table 2 provides quantitative metrics for reconstruction quality. In the supplement, we provide 3D visualizations of the reconstructed point clouds.

From Figure 5, we observe that AO SL produces depth

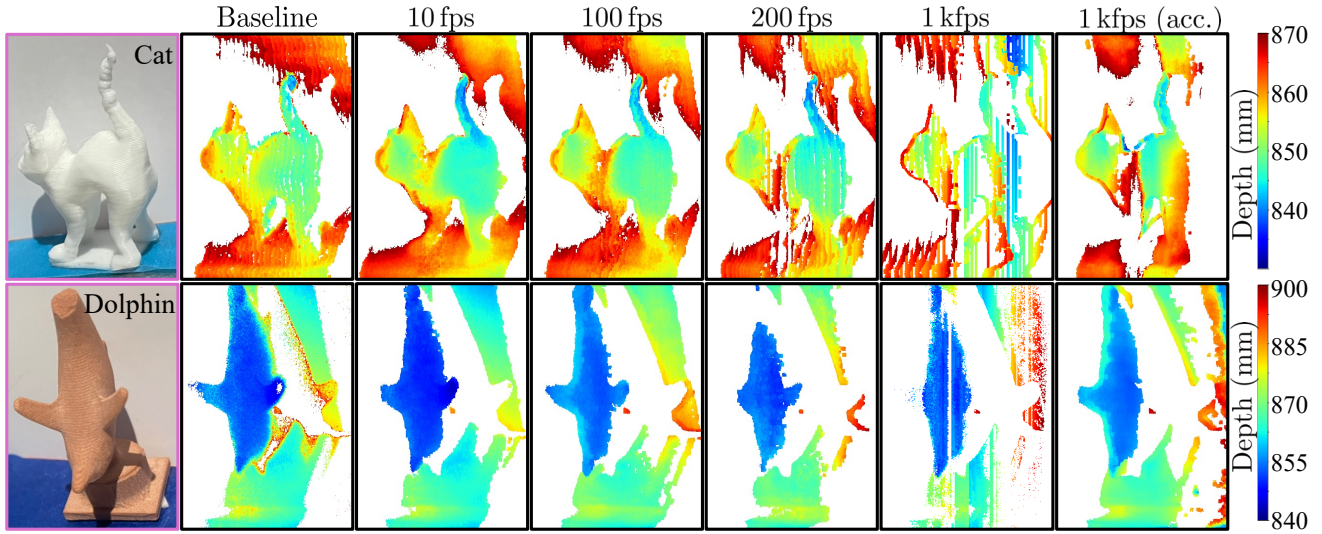


Figure 5. Depth scanning of static scenes at different scan rates. We scan a cat (top) and a dolphin (bottom) figurine, using the proposed AO SL system, at scan rates of 10 fps, 100 fps, 200 fps, and 1 kfps. We use Galvo-based SL at 10 fps as the baseline for comparison. In Table 2, we quantify reconstruction quality. Our proposed AO SL system reconstructs depth with high fidelity, but quality worsens as frame rate increases. At high frame rates, the event camera drops events randomly as the number of events exceeds its readout bandwidth.

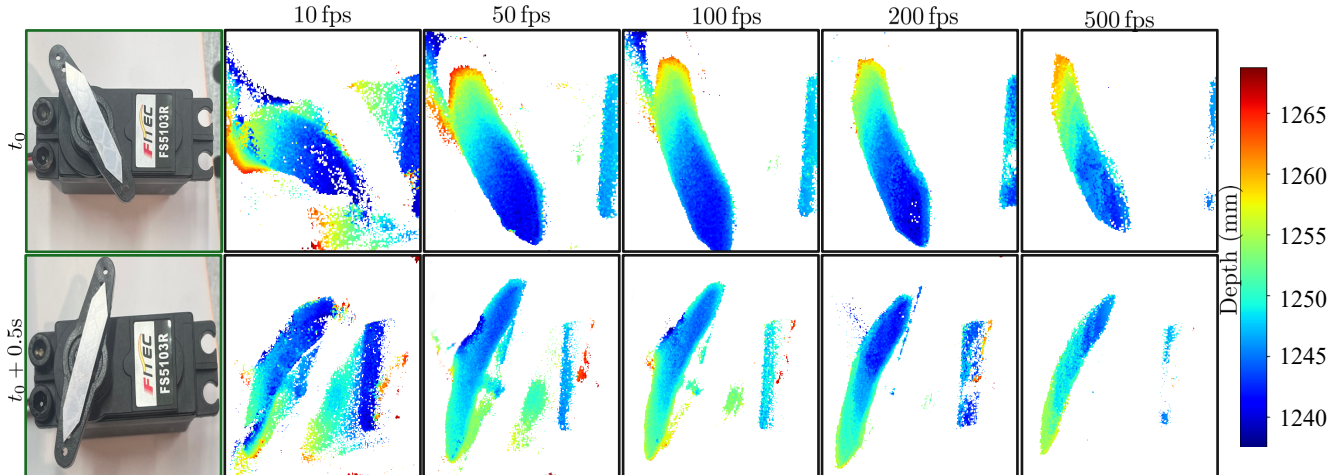


Figure 6. Depth scanning of a servo motor rotating at 70 rpm. Each row displays two frames (corresponding to times t_0 and $t_0 + 0.5$ s) from scans obtained at scan rates of 10 fps, 50 fps, 100 fps, 200 fps, and 500 fps. At 10 fps, the scan does not produce a correct depth map, as the rapid motion in the scene exceeds the scan rate. At 50 fps, the scan provides a depth map that is more accurate but still exhibits motion blur (visible more clearly in the supplementary video). As scan rates increase to 500 fps, the depth maps become progressively more accurate.

results that are nearly identical to Galvo-based SL at low scanning rates. As scanning rate increases, reconstruction quality progressively deteriorates. This loss of reconstruction quality occurs due to two main reasons: 1. Higher scan rates result in decreased exposure time and signal-to-noise ratio, which in turn cause a lot more noise events to be triggered. 2. The linewidth produced by the AO device is around 10 pixels, and thus each line triggers events at multiple sensor columns. At high scan rates, this increased number of events saturates the event camera, making it randomly lose

some events (columns) and causing the missing stripes. At 1 kfps, the number of missing columns due to the second issue becomes significant. To mitigate this issue, we experimented with accumulating multiple frames (“acc.” in Figure 5 and Table 2), effectively simulating a higher bandwidth event camera. We observe that doing so produces complete depth scans. This effect is scene-dependent, and sparse scenes as in Figure 1 do not suffer from reduced reconstruction quality due to limited readout bandwidth.

In Table 2, we quantify the 3D reconstruction fidelity

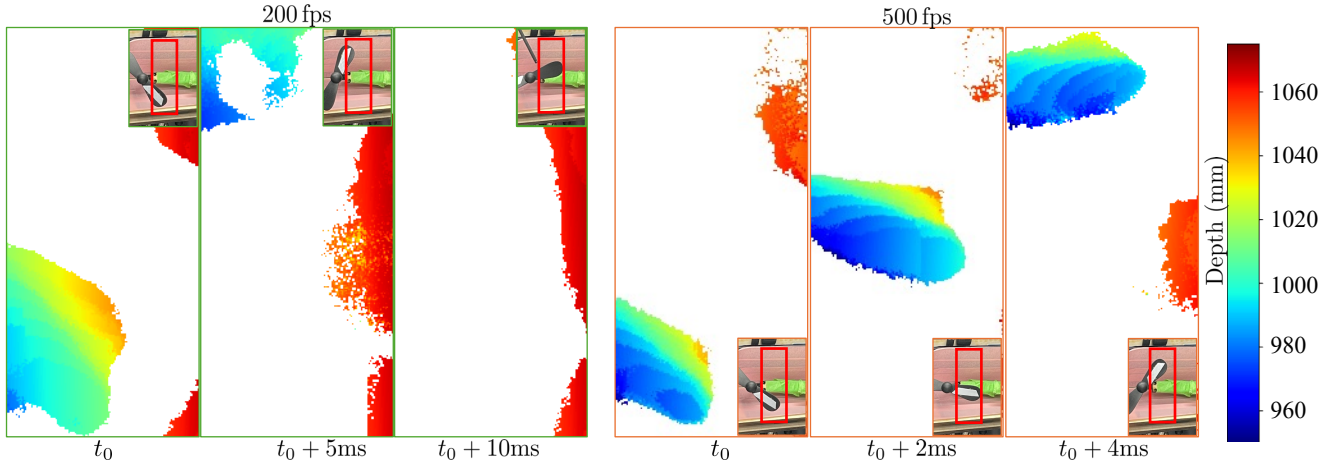


Figure 7. Depth scanning of a fan rotating at 1800 rpm. The left column displays three consecutive depth scans captured at a scan rate of 200 fps. The right column shows the same for a higher scan rate of 500 fps. The depth maps show significantly more motion blur on the blade area at 200 fps than at 500 fps. The red regions are from the background reference plane, used for calibration. The insets show the approximate orientation of the fan blade, and the area inside the red box is the scanned region.

using chamfer distance, precision, recall, and F1 score. As the frame rate increases, all metrics deteriorate as expected. With accumulation, the metrics improve significantly.

5.2. Dynamic scene results

We characterized the performance of our AO SL device on two dynamic scenes: 1. a servo motor rotating at 70 rpm, which we show in Figure 6 (blade diameter is 35 mm); 2. a high-speed fan rotating at 1800 rpm, which we show in Figure 7 (blade diameter is 72 mm). As the fan blades are dark and we are scanning at very low exposures, we used retroreflectors to increase reflectivity.

For the 70 rpm servo, Figure 6 shows results for five scan rates: 10 fps, 50 fps, 100 fps, 200 fps, and 500 fps. The servo is rotating clockwise, and we show depth scans of two frames separated by 0.5 s. The RGB images show the orientation of the blade and the region where the reflectors are located. At 10 fps, the depth maps suffer from significant blur. At 50 fps, the depth maps improve significantly but still have motion blur (seen as increased blade thickness). The results become increasingly sharp as the scan rate increases. The video results in the supplement show continuous depth scans of the dynamic scene at all scan rates.

For the more challenging fan rotating at 1800 rpm, Figure 7 shows results at scan rates of 200 fps and 500 fps. The fan blade has considerably more motion blur at 200 fps than at 500 fps. The former case is representative of the expected performance of the previous state of the art by Dashpute et al. [11], who reported scan rates of 250 fps.

5.3. Adaptive depth scanning

As we mentioned in Section 4, the event sensor can capture only up to 1 k frames per second at megapixel resolution. In

a dynamic scene, typically depth changes only at few pixels corresponding to the moving objects. Therefore, one way to increase scan rate beyond the sensor’s theoretical full-frame rate is to perform adaptive scanning, where we only scan the regions where the depth has changed. Muglikar et al. [36] have previously demonstrated that adaptive scanning of only regions of interest improves spatial and temporal resolution. As in their work, we can illuminate only the important regions of the scene to reduce the event camera bandwidth and increase overall scan rate.

Our AO light scanning device can illuminate any arbitrary line with high fidelity and at the same rate as ultrasound frequency, making it well-suited for adaptive scanning. The AO device can send each illumination photon toward any specific line using Equation (6). While a Galvo mirror can also perform adaptive scanning, it is slow and cannot scan beyond the frame rate of the event sensor. Further, during the mechanical mirror rotation to move the laser from one line location to another, the laser continues to illuminate the in-between region and generate events, making adaptive scanning less effective at suppressing unnecessary events.

To demonstrate adaptive scanning, we show in Figure 8 a scene comprising two orange knobs at two different depths. We scanned the positions of only these knobs with the Galvo mirror device and the AO device at various scan rates. From the plot in Figure 8, we observe that the Galvo mirror device produces accurate depth at low frame rates. However, as the frame rate increases, the depth error increases significantly. By contrast, the accuracy of the AO device remains fairly constant, even at a very high scan rate.

To better understand this performance difference, we show captured event data in Figure 8(b), with color representing the time stamp of the events. In the supplement,

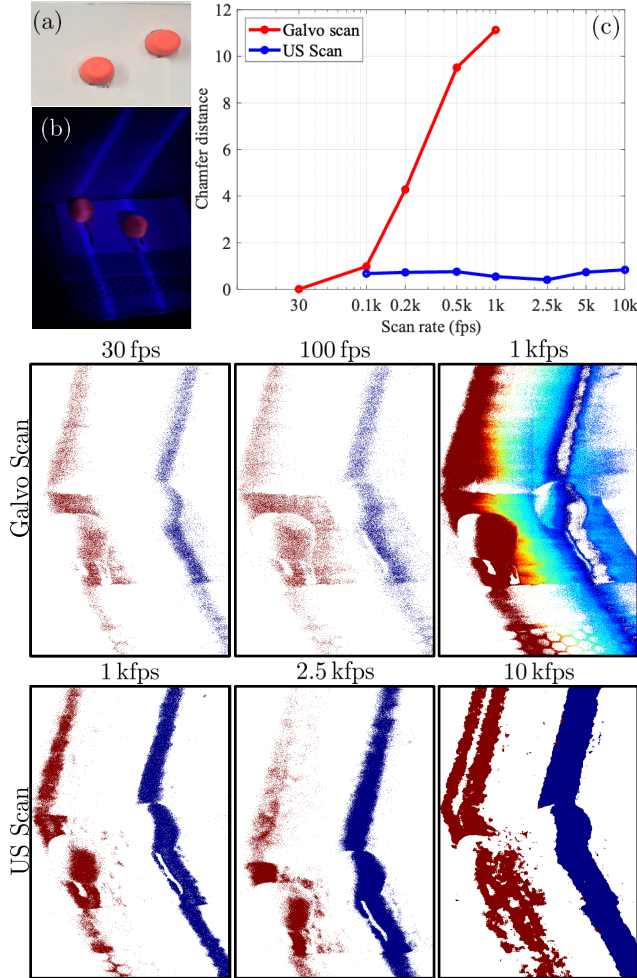


Figure 8. Adaptive scanning of two regions of interest (orange knobs) in a scene shown in (a). We aim to illuminate only two light planes corresponding to the knobs, as depicted in (b) to compute the depths of these knobs. We can create this adaptive illumination with both the Galvo device and the AO device. In (c), we show the depth error measured for these knobs when we scan with the Galvo device vs the AO device. At low scan rates, the Galvo mirror device is effective at adaptively scanning only the knobs. However, as the scan rate increases, its performance deteriorates. This deterioration is natural to the Galvo mirror as it mechanically rotates the beam from one line location to another location, invariably illuminating the regions in between. At high speed, the amount of time the region in between lines is illuminated increases, decreasing its performance. By contrast, our AO device can place lines at only the regions of interest even while operational at speeds of 10 kfps, resulting in effective adaptive scanning.

we provide the event stream videos to show the behavior more clearly. From this data, we observe that at low scan rates, the Galvo mirror device projects most of the laser’s light output to the two lines of interest, but as the scan rate increases, it projects most of the light output incorrectly to the region between the two lines. By contrast, the AO device

always projects all light at only the two lines of interest.

We note that we could not scan the Galvo mirror device beyond a 1 kHz rate, as that is the physical limit for these devices. For our AO device, we could theoretically go up to 1 MHz to scan two lines (given that the transducer operates at 2 MHz). However, as the frame rate increases, the amount of light decreases, and we noticed empirically that at 20 kHz the amount of light reaching the event sensor is below its detection threshold. Therefore, though theoretically we can scan up to 1 MHz adaptively, practically, we are limited by our laser power to a 10 kHz scan rate, which is still $10\times$ higher than the event camera’s full-frame frame rate.

We strongly encourage readers to explore the accompanying supplementary videos for a comprehensive visualization of these results

6. Discussion and conclusion

We designed an acousto-optic device to scan light planes at unprecedented rates of up to 2 MHz, and combined it with an event camera to perform swept-plane structured light. This combination allowed us to achieve full-frame 3D scanning at 1000 fps, $3\text{--}4\times$ faster than the state of the art [11]. However, our method has a few limitations, some of which can be addressed by modifications to the prototype, whereas other point towards future research directions. On the first front, similar to Pediredla et al. [44], the acousto-optic device has a small aperture, which due to diffraction results in large linewidths and thus reduced spatial and depth resolution. Using a transmission medium where the speed of sound is faster than in water would increase the ultrasound wavelength and hence aperture size, addressing this issue. Additionally, our laser has a low emission power ($\approx 1\text{ mW}$), necessitating light accumulation over multiple scans at higher frame rates and the use of a large aperture lens, which reduces the scene’s depth-of-field. Using a better laser would mitigate both issues. In terms of more fundamental limitations, the limited bandwidth of the event camera is the bottleneck preventing a faster 3D scanning rate, creating a gap of three orders of magnitude with the light scanning rate. Closing this gap requires research into sensors that not only have drastically larger readout bandwidths, but also can operate at drastically shorter exposure times. Single-photon avalanche diodes are a promising option to this end, as they have already been shown to be suitable for ultra-wideband operation [65] and structured light under minuscule exposures [57]. Lastly, our system creates opportunities for combinations with other imaging modalities that use additional dimensions of light (e.g., polarization, wavelength) to further enhance robustness against effects such as specularly, glare, and scattering.

References

- [1] Mohammad Abdo, Vlad Badilita, and Jan Korvink. Spatial scanning hyperspectral imaging combining a rotating slit with a dove prism. *Optics Express*, 27(15):20290–20304, 2019. 2
- [2] Supreeth Achar, Joseph R. Bartels, William L. 'Red' Whitaker, Kiriakos N. Kutulakos, and Srinivasa G. Narasimhan. Epipolar time-of-flight imaging. *ACM Trans. Graph.*, 36(4), 2017. 2
- [3] Jared Beller and Linbo Shao. Acousto-optic modulators integrated on-chip. *Light: Science & Applications*, 11(1):1–2, 2022. 2
- [4] Jean-Yves Bouguet and Pietro Perona. 3D photography using shadows in dual-space geometry. *International Journal of Computer Vision*, 35:129–149, 1999. 4, 5, 2
- [5] Christian Brandli, Thomas A Mantel, Marco Hutter, Markus A Höpflinger, Raphael Berner, Roland Siegwart, and Tobi Delbruck. Adaptive pulsed laser line extraction for terrain reconstruction using a dynamic vision sensor. *Frontiers in neuroscience*, 7:275, 2014. 2
- [6] Dalit Caspi, Nahum Kiryati, and Joseph Shamir. Range imaging with adaptive color structured light. *IEEE Transactions on Pattern Analysis and Machine Intelligence*, 20(5):470–480, 1998. 3
- [7] Maysamreza Chamanzar, Matteo Giuseppe Scopelliti, Julien Bloch, Ninh Do, Minyoung Huh, Dongjin Seo, Jillian Iafrazi, Vikaas S Sohal, Mohammad-Reza Alam, and Michel M Maharbiz. Ultrasonic sculpting of virtual optical waveguides in tissue. *Nature communications*, 10(1):1–10, 2019. 2
- [8] Dorian Chan, Srinivasa G Narasimhan, and Matthew O'Toole. Holocurtains: Programming light curtains via binary holography. In *Proceedings of the IEEE/CVF Conference on Computer Vision and Pattern Recognition*, pages 17886–17895, 2022. 2
- [9] Sreenithy Chandran, Hiroyuki Kubo, Tomoki Ueda, Takuya Funatomi, Yasuhiro Mukaigawa, and Suren Jayasuriya. Slope disparity gating: System and applications. *IEEE Transactions on Computational Imaging*, 8:317–332, 2022. 2
- [10] Maxim N Cherkashin, Carsten Brenner, Georg Schmitz, and Martin R Hofmann. Transversally travelling ultrasound for light guiding deep into scattering media. *Communications Physics*, 3(1):1–11, 2020. 2
- [11] Aniket Dashpute, Jiazhang Wang, James Taylor, Oliver Coscairt, Ashok Veeraraghavan, and Florian Willomitzer. Event-based Motion-Robust Accurate Shape Estimation for Mixed Reflectance Scenes. *arXiv preprint arXiv:2311.09652*, 2023. 2, 3, 7, 8
- [12] Vladislav Gavryusev, Giuseppe Sancataldo, Pietro Ricci, Alberto Montalbano, Chiara Fornetto, Lapo Turrini, Annunziata Laurino, Luca Pesce, Giuseppe de Vito, Natascia Tiso, et al. Dual-beam confocal light-sheet microscopy via flexible acousto-optic deflector. *Journal of biomedical optics*, 24(10):106504, 2019. 2
- [13] Milton S Gottlieb. Acousto-optic tunable filters. In *Design and fabrication of acousto-optic devices*, pages 197–283. CRC Press, 2021. 2
- [14] Mohit Gupta, Amit Agrawal, Ashok Veeraraghavan, and Srinivasa G Narasimhan. Structured light 3d scanning in the presence of global illumination. In *CVPR 2011*, pages 713–720. IEEE, 2011. 2, 3
- [15] Jin Han, Chu Zhou, Peiqi Duan, Yehui Tang, Chang Xu, Chao Xu, Tiejun Huang, and Boxin Shi. Neuromorphic camera guided high dynamic range imaging. In *Proceedings of the IEEE/CVF Conference on Computer Vision and Pattern Recognition*, pages 1730–1739, 2020. 2
- [16] Chen Haoyu, Teng Minggui, Shi Boxin, Wang YIzhou, and Huang Tiejun. Learning to deblur and generate high frame rate video with an event camera. *arXiv preprint arXiv:2003.00847*, 2020. 2
- [17] Ching-Pai Hsu, Boda Li, Braulio Solano-Rivas, Amar R Gohil, Pak Hung Chan, Andrew D Moore, and Valentina Donzella. A review and perspective on optical phased array for automotive lidar. *IEEE Journal of Selected Topics in Quantum Electronics*, 27(1):1–16, 2020. 2
- [18] Peisen S Huang, Chengping Zhang, and Fu-Pen Chiang. High-speed 3-d shape measurement based on digital fringe projection. *Optical engineering*, 42(1):163–168, 2003. 3
- [19] Dawoon Jeong, Hansol Jang, Min Uk Jung, and Chang-Seok Kim. Angular resolution variable fmcw lidar with acousto-optic deflector. In *Imaging Systems and Applications*, pages ITh4D–3. Optica Publishing Group, 2022. 2
- [20] SeungYeon Kang, Martí Duocastella, and Craig B Arnold. Variable optical elements for fast focus control. *Nature Photonics*, 14(9):533–542, 2020. 2
- [21] Yasin Karimi, Matteo Giuseppe Scopelliti, Ninh Do, Mohammad-Reza Alam, and Maysamreza Chamanzar. In situ 3d reconfigurable ultrasonically sculpted optical beam paths. *Optics express*, 27(5):7249–7265, 2019. 2
- [22] Byung-Sub Kim, Steve Gibson, and Tsu-Chin Tsao. Adaptive control of a tilt mirror for laser beam steering. In *Proceedings of the 2004 American Control Conference*, pages 3417–3421. IEEE, 2004. 2
- [23] Hanme Kim, Ankur Handa, Ryad Benosman, Sio-Hoi Ieng, and Andrew J Davison. Simultaneous mosaicing and tracking with an event camera. *J. Solid State Circ.*, 43:566–576, 2008. 2
- [24] Hiroyuki Kubo, Suren Jayasuriya, Takafumi Iwaguchi, Takuya Funatomi, Yasuhiro Mukaigawa, and Srinivasa G Narasimhan. Programmable non-epipolar indirect light transport: Capture and analysis. *IEEE Transactions on Visualization and Computer Graphics*, 27(4):2421–2436, 2019. 2
- [25] Douglas Lanman and Gabriel Taubin. Build your own 3d scanner: 3d photography for beginners. In *ACM siggraph 2009 courses*, pages 1–94. ACM, 2009. 4, 5, 2
- [26] T Leroux, S-H Ieng, and Ryad Benosman. Event-based structured light for depth reconstruction using frequency tagged light patterns. *arXiv preprint arXiv:1811.10771*, 2018. 3
- [27] David B Lindell, Gordon Wetzstein, and Matthew O'Toole. Wave-based non-line-of-sight imaging using fast fk migration. *ACM Transactions on Graphics (ToG)*, 38(4):1–13, 2019. 2
- [28] Han-Chao Liu, Fang-Lue Zhang, David Marshall, Luping Shi, and Shi-Min Hu. High-speed video generation with an event camera. *The Visual Computer*, 33:749–759, 2017. 2
- [29] Qiyu Liu, Huan Li, and Mo Li. Electromechanical brillouin scattering in integrated optomechanical waveguides. *Optica*, 6(6):778–785, 2019. 2

- [30] Xiaochun Liu, Ibón Guillén, Marco La Manna, Ji Hyun Nam, Syed Azer Reza, Toan Huu Le, Adrian Jarabo, Diego Gutierrez, and Andreas Velten. Non-line-of-sight imaging using phasor-field virtual wave optics. *Nature*, 572(7771):620–623, 2019. 2
- [31] Ashish Rao Mangalore, Chandra Sekhar Seelamantula, and Chetan Singh Thakur. Neuromorphic fringe projection profilometry. *IEEE Signal Processing Letters*, 27:1510–1514, 2020. 3
- [32] Julien NP Martel, Jonathan Müller, Jörg Conradt, and Yulia Sandamirskaya. An active approach to solving the stereo matching problem using event-based sensors. In *2018 IEEE International Symposium on Circuits and Systems (ISCAS)*, pages 1–5. IEEE, 2018. 3
- [33] Nathan Matsuda, Oliver Cossairt, and Mohit Gupta. Mc3d: Motion contrast 3d scanning. In *2015 IEEE International Conference on Computational Photography (ICCP)*, pages 1–10. IEEE, 2015. 2, 3
- [34] Aongus McCarthy, Nils J Krichel, Nathan R Gemmell, Ximing Ren, Michael G Tanner, Sander N Dorenbos, Val Zwiller, Robert H Hadfield, and Gerald S Buller. Kilometer-range, high resolution depth imaging via 1560 nm wavelength single-photon detection. *Optics express*, 21(7):8904–8915, 2013. 2
- [35] Manasi Muglikar, Guillermo Gallego, and Davide Scaramuzza. ESL: Event-based structured light. In *2021 International Conference on 3D Vision (3DV)*, pages 1165–1174. IEEE, 2021. 2, 3, 5
- [36] Manasi Muglikar, Diederik Paul Moeys, and Davide Scaramuzza. Event guided depth sensing. In *2021 International Conference on 3D Vision (3DV)*, pages 385–393. IEEE, 2021. 2, 3, 7
- [37] Srinivasa Narasimhan, Supreeth Achar, Kiriakos Kutulakos, Joe Bartels, and William Whittaker. Method for epipolar time of flight imaging, 2020. US Patent App. 16/468,617. 2
- [38] Matthew O’Toole, Ramesh Raskar, and Kiriakos N Kutulakos. Primal-dual coding to probe light transport. *ACM Trans. Graph.*, 31(4):39–1, 2012.
- [39] Matthew O’Toole, Supreeth Achar, Srinivasa G Narasimhan, and Kiriakos N Kutulakos. Homogeneous codes for energy-efficient illumination and imaging. *ACM Transactions on Graphics (ToG)*, 34(4):1–13, 2015. 2
- [40] Matthew O’Toole, David B Lindell, and Gordon Wetzstein. Confocal non-line-of-sight imaging based on the light-cone transform. *Nature*, 555(7696):338–341, 2018. 2
- [41] Liyuan Pan, Cedric Scheerlinck, Xin Yu, Richard Hartley, Miaomiao Liu, and Yuchao Dai. Bringing a blurry frame alive at high frame-rate with an event camera. In *Proceedings of the IEEE/CVF Conference on Computer Vision and Pattern Recognition*, pages 6820–6829, 2019. 2
- [42] Liyuan Pan, Richard Hartley, Cedric Scheerlinck, Miaomiao Liu, Xin Yu, and Yuchao Dai. High frame rate video reconstruction based on an event camera. *IEEE Transactions on Pattern Analysis and Machine Intelligence*, 44(5):2519–2533, 2020. 2
- [43] Adithya Pediredla, Akshat Dave, and Ashok Veeraraghavan. Snlos: Non-line-of-sight scanning through temporal focusing. In *2019 IEEE International Conference on Computational Photography (ICCP)*, pages 1–13. IEEE, 2019. 2
- [44] Adithya Pediredla, Srinivasa G Narasimhan, Maysamreza Chamanzar, and Ioannis Gkioulekas. Megahertz Light Steering Without Moving Parts. In *Proceedings of the IEEE/CVF Conference on Computer Vision and Pattern Recognition*, pages 1–12, 2023. 2, 3, 4, 8
- [45] Jeffrey L Posdamer and Martin D Altschuler. Surface measurement by space-encoded projected beam systems. *Computer graphics and image processing*, 18(1):1–17, 1982. 3
- [46] Christopher V Poulton, Matthew J Byrd, Benjamin Moss, Erman Timurdogan, Ron Millman, and Michael R Watts. 8192-element optical phased array with 100° steering range and flip-chip cmos. In *CLEO: QELS-Fundamental Science*, pages JTh4A–3. Optical Society of America, 2020. 2
- [47] Henri Rebecq, Timo Horstschäfer, Guillermo Gallego, and Davide Scaramuzza. Evo: A geometric approach to event-based 6-dof parallel tracking and mapping in real time. *IEEE Robotics and Automation Letters*, 2(2):593–600, 2016. 2
- [48] Joshua Rodriguez, Braden Smith, Brandon Hellman, Adley Gin, Alonzo Espinoza, and Yuzuru Takashima. Multi-beam and single-chip lidar with discrete beam steering by digital micromirror device. In *Physics and Simulation of Optoelectronic Devices XXVI*, pages 89–94. SPIE, 2018. 2
- [49] Cedric Scheerlinck, Nick Barnes, and Robert Mahony. Continuous-time intensity estimation using event cameras. In *Asian Conference on Computer Vision*, pages 308–324. Springer, 2018. 2
- [50] Xiaobing Shang, Jin-Yi Tan, Oliver Willekens, Jelle De Smet, Pankaj Joshi, Dieter Cuyper, Esmá Islamaj, Jeroen Beeckman, Kristiaan Neyts, Michael Vervaeke, et al. Electrically controllable liquid crystal component for efficient light steering. *IEEE Photonics Journal*, 7(2):1–13, 2015. 2
- [51] Prasan Shedligeri and Kaushik Mitra. Photorealistic image reconstruction from hybrid intensity and event-based sensor. *Journal of Electronic Imaging*, 28(6):063012–063012, 2019. 2
- [52] Braden Smith, Brandon Hellman, Adley Gin, Alonzo Espinoza, and Yuzuru Takashima. Single chip lidar with discrete beam steering by digital micromirror device. *Optics Express*, 25(13):14732–14745, 2017. 2
- [53] Qi Wang Song, Xu-Ming Wang, Rebecca Bussjager, and Joseph Osman. Electro-optic beam-steering device based on a lanthanum-modified lead zirconate titanate ceramic wafer. *Applied optics*, 35(17):3155–3162, 1996. 2
- [54] Lin Sun, Jin-ha Kim, Chiou-hung Jang, Dechang An, Xuejun Lu, Qingjun Zhou, John Martin Taboada, Ray T Chen, Jeffery J Maki, Suning Tang, et al. Polymeric waveguide prism-based electro-optic beam deflector. *Optical Engineering*, 40(7):1217–1222, 2001. 2
- [55] Lei Sun, Christos Sakaridis, Jingyun Liang, Qi Jiang, Kailun Yang, Peng Sun, Yaozu Ye, Kaiwei Wang, and Luc Van Gool. Event-based fusion for motion deblurring with cross-modal attention. In *European conference on computer vision*, pages 412–428. Springer, 2022. 2
- [56] Lei Sun, Christos Sakaridis, Jingyun Liang, Peng Sun, Jiezhong Cao, Kai Zhang, Qi Jiang, Kaiwei Wang, and Luc

- Van Gool. Event-based frame interpolation with ad-hoc deblurring. In *Proceedings of the IEEE/CVF Conference on Computer Vision and Pattern Recognition*, pages 18043–18052, 2023. 2
- [57] Varun Sundar, Sizhuo Ma, Aswin C Sankaranarayanan, and Mohit Gupta. Single-photon structured light. In *Proceedings of the IEEE/CVF Conference on Computer Vision and Pattern Recognition*, pages 17865–17875, 2022. 2, 8
- [58] Chen S Tsai. *Guided-wave acousto-optics: interactions, devices, and applications*. Springer Science & Business Media, 2013. 2
- [59] Stepan Tulyakov, Daniel Gehrig, Stamatios Georgoulis, Julius Erbach, Mathias Gehrig, Yuanyou Li, and Davide Scaramuzza. Time lens: Event-based video frame interpolation. In *Proceedings of the IEEE/CVF conference on computer vision and pattern recognition*, pages 16155–16164, 2021. 2
- [60] Stepan Tulyakov, Alfredo Bochicchio, Daniel Gehrig, Stamatios Georgoulis, Yuanyou Li, and Davide Scaramuzza. Time lens++: Event-based frame interpolation with parametric non-linear flow and multi-scale fusion. In *Proceedings of the IEEE/CVF Conference on Computer Vision and Pattern Recognition*, pages 17755–17764, 2022. 2
- [61] Tomoki Ueda, Hiroyuki Kubo, Suren Jayasuriya, Takuya Funatomi, and Yasuhiro Mukaigawa. Slope disparity gating using a synchronized projector-camera system. In *2019 IEEE International Conference on Computational Photography (ICCP)*, pages 1–9. IEEE, 2019. 2
- [62] Jian Wang, Joseph Bartels, William Whittaker, Aswin C Sankaranarayanan, and Srinivasa G Narasimhan. Programmable triangulation light curtains. In *Proceedings of the European Conference on Computer Vision (ECCV)*, pages 19–34, 2018. 2
- [63] Xiangru Wang, Liang Wu, Caidong Xiong, Man Li, Qinggui Tan, Jiyang Shang, Shuanghong Wu, and Qi Qiu. Agile laser beam deflection with high steering precision and angular resolution using liquid crystal optical phased array. *IEEE Transactions on Nanotechnology*, 17(1):26–28, 2016. 2
- [64] Zihan Wang, Jie Cao, Qun Hao, Fanghua Zhang, Yang Cheng, and Xianyue Kong. Super-resolution imaging and field of view extension using a single camera with risley prisms. *Review of Scientific Instruments*, 90(3):033701, 2019. 2
- [65] Mian Wei, Sotiris Nousias, Rahul Gulve, David B Lindell, and Kiriakos N Kutulakos. Passive ultra-wideband single-photon imaging. In *Proceedings of the IEEE/CVF International Conference on Computer Vision*, pages 8135–8146, 2023. 8
- [66] Shumian Xin, Sotiris Nousias, Kiriakos N Kutulakos, Aswin C Sankaranarayanan, Srinivasa G Narasimhan, and Ioannis Gkioulekas. A theory of fermat paths for non-line-of-sight shape reconstruction. In *Proceedings of the IEEE/CVF conference on computer vision and pattern recognition*, pages 6800–6809, 2019. 2
- [67] Fang Xu, Lei Yu, Bishan Wang, Wen Yang, Gui-Song Xia, Xu Jia, Zhendong Qiao, and Jianzhuang Liu. Motion deblurring with real events. In *Proceedings of the IEEE/CVF International Conference on Computer Vision*, pages 2583–2592, 2021. 2
- [68] Jiawen Xu and Jiong Tang. Tunable prism based on piezoelectric metamaterial for acoustic beam steering. *Applied Physics Letters*, 110(18):181902, 2017. 2
- [69] Donghai Yang, Yifan Liu, Qingjiu Chen, Meng Chen, Shaodong Zhan, Nim-kwan Cheung, Ho-Yin Chan, Zhidong Wang, and Wen Jung Li. Development of the high angular resolution 360° lidar based on scanning mems mirror. *Scientific Reports*, 13(1):1540, 2023. 2
- [70] Zejie Yu and Xiankai Sun. Gigahertz acousto-optic modulation and frequency shifting on etchless lithium niobate integrated platform. *ACS Photonics*, 8(3):798–803, 2021. 2
- [71] Limeng Zhang, Hongguang Zhang, Jihua Chen, and Lei Wang. Hybrid deblur net: Deep non-uniform deblurring with event camera. *IEEE Access*, 8:148075–148083, 2020. 2

Structured light with a million light planes per second

Supplementary Material

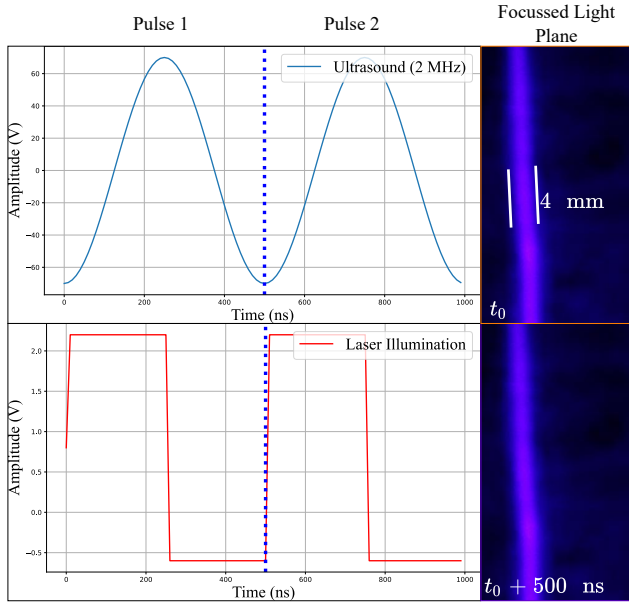


Figure 9. Stationary light plane creation. The system toggles illumination on and off every 500 ns, keeping the light plane stationary instead of moving with the speed of sound. The thickness of the focused line is 4 mm

7. How to Keep the Light Plane Stationary Instead of Moving at the Speed of Sound in Water?

To keep the light plane stationary, rather than moving at the speed of sound along with the sculpted lenses, we synchronize the laser pulses with the frequency of the ultrasound wave. The ultrasound wave oscillates sinusoidally at 2 MHz, and we pulse the laser at the same frequency (2 MHz), as we show in the duty cycle diagram in Figure 9. This synchronization ensures the light plane remains stationary and unaffected by the movement of the sculpted lenses.

The method activates the laser each time a new sound wave reaches a specific point x in the medium, and deactivates it as the wave moves past x . By timing the laser pulses perfectly with the propagation of the sound wave, the system keeps the light plane stationary. Figure 9 visualizes this method. The laser pulses every 500 ns, corresponding to the 2 MHz pulsing frequency. This sequence stabilizes the light plane at a fixed position, preventing it from traveling through the medium.

8. How is the Light Plane Moved at a Certain Speed?

In Section 7, we demonstrated how to position a light plane at a stationary location. In this section, we examine how the pulsing frequency and delay influence the light plane's position and enable its controlled movement.

Assuming the laser continues pulsing at a frequency of 2 MHz, we introduce a time delay in the pulse, which shifts the illuminated spot of the light plane. We can precisely control this time delay by adjusting the phase of the laser pulse relative to the ultrasound wave. Figure 10 visualizes how varying the pulsing delay affects the position of the light plane. It demonstrates the direct relationship between phase adjustments and the spatial shift in illumination. We can express the time delay in illumination mathematically as:

$$\phi = \omega_{us}t \implies t_{\text{delay}} = \frac{\phi}{\omega_{us}}, \quad (7)$$

where ϕ is the phase delay, ω_{us} is the angular frequency of the ultrasound, and t_{delay} is the resulting time delay. By adjusting this delay, we can control the location at which the light plane is illuminated.

If we define the phase delay ϕ as a time-varying function, such as $\phi(t) = \omega_{\text{spf}}t$, where ω_{spf} represents the frequency of the swept plane, we can dynamically move the light plane at a desired speed. Using this formulation, we can sweep the light plane across space at a controlled speed determined by ω_{spf} .

9. How to Position and Oscillate Between Arbitrary Locations at Desired Speeds?

In Section 7, we explained how to position a light plane at a specific location by adjusting the delay in illuminations, and in Section 8, we described how to move these lines at desirable speeds. In this section, we detail how to illuminate two specific light planes at distinct locations of interest (Figure 11(a)).

We assume we want to position two light planes, LP_1 and LP_2 , at delays of 0 ns and 250 ns, respectively, when pulsing the laser. To determine these time delay locations, we adjust the phase of the laser pulse as $\phi = \omega_{us}t_{\text{delay}}$ from Equation (7). Creating a suitable waveform is straightforward, as we show in Figure 11(b, c). These waveforms position the light planes at the desired locations, as we show in Figure 11(d, e).

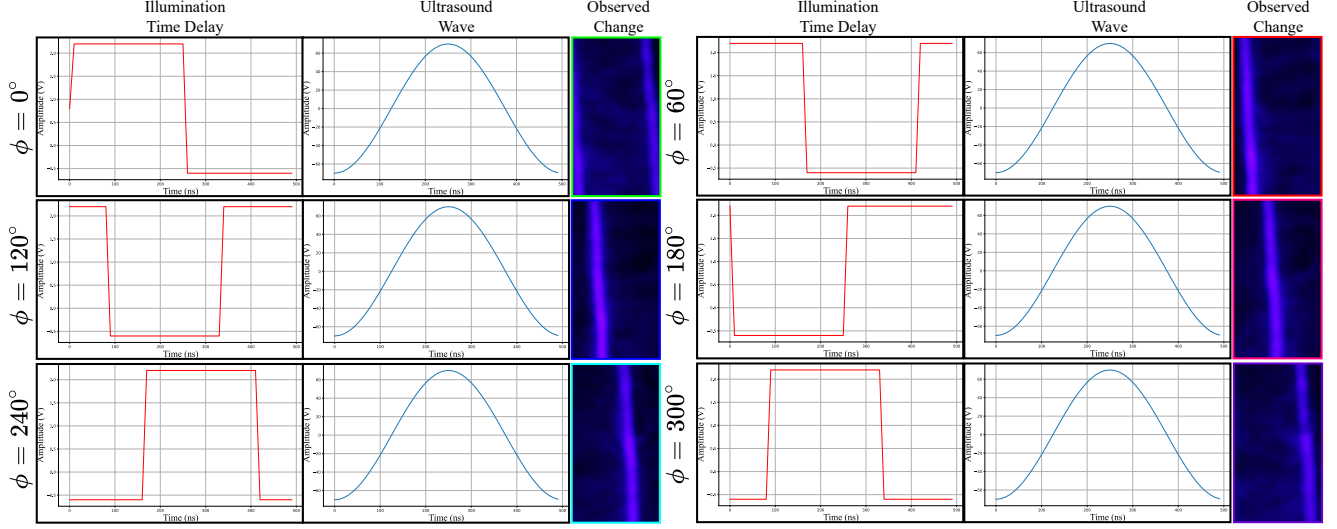


Figure 10. Effect of time delay in illumination pulses for achieving various light plane positions.

9.1. How do we control the oscillation speed between LP_1 and LP_2 ?

To control the speed of oscillation between these planes, we repeat the pulse with delay d_i multiple times before transitioning to d_{i+1} . This repetition adjusts the oscillation speed as needed.

For a general scenario, where n_l represents the number of lines of interest and f_d represents the desired oscillation speed, we calculate the number of pulse repetitions P_r as follows:

$$P_r = \frac{f_{us}}{n_l \times f_d}. \quad (8)$$

From this equation, using $f_{us} = 2$ MHz, desired oscillation frequency 10 kHz, and $n_l = 2$ lines of interest, we compute:

$$P_r = \frac{2 \times 10^6}{2 \times 10 \times 10^3} = 100. \quad (9)$$

This calculation indicates that the pulse with $d_1 = 0$ ns should repeat 100 times, followed by 100 repetitions of the pulse with $d_2 = 250$ ns, to achieve an oscillation speed of 10 kHz (10 kfps).

The laser pulse waveform is given by the ordered sequence:

$$\{\underbrace{d_1, d_1, \dots, d_1}_{P_r} \underbrace{d_2, d_2, \dots, d_2}_{P_r} \dots \underbrace{d_{n_l}, d_{n_l}, \dots, d_{n_l}}_{P_r}\}, \quad (10)$$

For a desired oscillation speed of 10 kfps with 2 light planes and 2 MHz transducer, the waveform is given by:

$$\{\underbrace{d_1, d_1, \dots, d_1}_{100 \text{ repeats}} \underbrace{d_2, d_2, \dots, d_2}_{100 \text{ repeats}}\}, \quad (11)$$

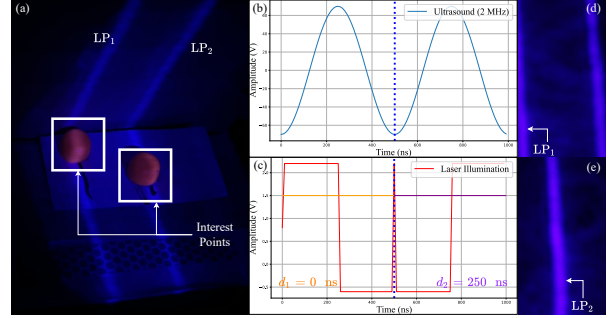


Figure 11. Arbitrary line placement. This example demonstrates positioning light planes at two locations, LP_1 and LP_2 (a). We achieve this by delaying the pulsing of the laser between consecutive pulses by $d_1 = 0^\circ \times \frac{180^\circ}{2\pi} / \omega_{us} = 0$ ns and $d_2 = 180^\circ \times \frac{180^\circ}{2\pi} / \omega_{us} = 250$ ns, where $\omega_{us} = 2\pi f_{us}$. With this configuration, the system illuminates the light planes LP_1 and LP_2 at a rate of 2 Mfps.

10. Reference planes for structured light

Our structured light scanner uses the classical swept-plane procedure [4, 25], which we visualize in Figure 12(a). Briefly, this procedure triangulates a 3D point for each event on the event camera, by backprojecting a ray from the pixel of the event camera and intersecting the ray with the light plane P that triggered this event.

The swept-plane method for structured light requires calibrating the light planes relative to the camera. To this end, we follow the procedure by Bouguet and Perona [4], which we visualize in Figure 12(b): We place two fixed approximately orthogonal reference planes in the scene (planes V and H), and calibrate their location and orientation with respect to the event camera. Then, we calibrate the scanned light planes using their linear intersections (lines λ_V and λ_H) with the two reference planes.

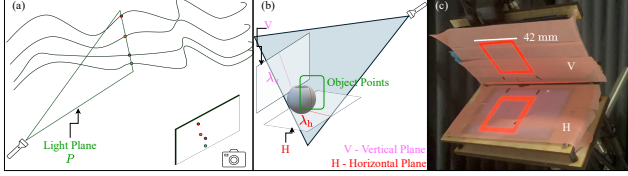


Figure 12. (a-b) Structured light by light plane sweeping. The image shows a light plane illuminating the scene. A camera observes the illuminated points, and the system retrieves depth information by triangulating the light plane. (c) Reference planes for calibration. We create the reference planes using an approximately orthogonal screen arrangement. We display blinking square patterns of size 42 mm on the screen to calibrate the reference planes with respect of the event camera.

To create reference planes that are easy to calibrate with respect to the event camera (which does not take conventional intensity measurements), we use two displays as we show in Figure 12(c). During the calibration, the displays project a blinking checkerboard pattern that creates events for the camera. During the calibration and scanning of the swept planes, we keep the displays off. As the displays are black, we apply translucent tape to make them reflective, ensuring that the camera captures events when the swept light plane hits the surface.

11. Hardware details

Section 11 shows the circuit diagram of our prototype: A dual-channel arbitrary waveform generator (AWG) drives both the transducer (T) and the pulsed laser (PL). Both channels operate at 2 MHz to maintain a stationary light plane. To move the light plane at a desired speed, we introduce a time-varying pulse delay $\phi(t)$, as we explained in Equation (7).

Table 3 lists the components we used to realize the hardware setup. The core components of the acousto-optic light scanning device are a water tank, transducers, and amplifiers. Additional components, such as the galvo-scanning hardware, are only for comparisons. The system requires a pulsed laser, the most expensive component, costing approximately USD 1750 apart from the signal generator. This is similar to Pediredla et al. [44]. Unlike their work, our design eliminates the need for a costly, high-power, high-bandwidth amplifier by shifting the steering control to the illumination side.

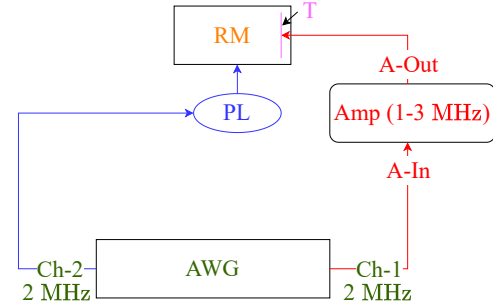


Figure 13. Circuit diagram of the hardware prototype. A two-channel arbitrary waveform generator (AWG) drives both the laser and the amplifier. Channel-1 (Ch-1) of the AWG connects to the Amp via the amplifier input (A-In) and then to the transducer (T) through the amplifier output (A-Out). The transducer (T) operates within the transparent medium (RM), sculpting the cylindrical lens. Channel-2 (Ch-2) of the AWG drives the pulsed laser (PL), which generates the light planes based on the mechanisms described in Section 7 and Section 8. The setup includes the following components: AWG - Arbitrary Waveform Generator, Ch-1 - Channel 1, Ch-2 - Channel 2, Amp - Amplifier (1 MHz–3 MHz), A-In - Amplifier Input, A-Out - Amplifier Output, T - Transducer, RM - Refractive Media, PL - Pulsed Laser.

Table 3. List of components for the hardware prototype.

component	manufacturer
water tank	B01K8WDE4I, Amazon.com, Inc.
transducers	P 12.7 mm-12.7 mm-1 mm-855-WFB, APC International, Ltd (Item No: 1976)
amplifiers	Generic 1 MHz–3 MHz Amplifier with 50 W output (available on Ebay)
signal generators(AWG)	SDG1032X, Siglent Tech.
Q-switched laser	Thorlabs NPL45B
40 mm convex lens	Thorlabs LA1274
galvo	GVS-211, Thorlabs Inc.
event camera	Prophesee, IMX636 sensor